

Towards Efficient Prompt-based Continual Learning in Distributed Medical AI

Gyutae Oh

Department of Electrical and Computer Engineering
Sungkyunkwan University
Suwon, Republic of Korea
alswo740012@g.skku.edu

Jitae Shin[†]

Department of Electrical and Computer Engineering
Sungkyunkwan University
Suwon, Republic of Korea
jtshin@skku.edu

Abstract—Modern AI models achieve state-of-the-art performance with large-scale, high-quality datasets; however, ethical, social, and institutional constraints in the medical domain severely restrict data sharing, rendering centralized learning nearly impossible. Each institution must incrementally update models using only local data. Traditional training overfits new samples and suffers from catastrophic forgetting, losing previously acquired knowledge. Medical data distributions also shift due to varying diagnostic equipment and demographics. Although continual learning (CL) has advanced, most methods address natural images, leaving medical-domain-specific CL underexplored. We propose a prompt-based continual learning (PCL) approach featuring a unified prompt pool with a minimal expansion strategy: by expanding and freezing a subset of prompts, our method reduces computational overhead, and a novel regularization term balances retention and adaptation. Experiments on three diabetic retinopathy datasets Aptos2019, LI2019, and Diabetic Retinopathy Detection show our model improves final classification accuracy by at least 10% and F1-score by 9 points over state-of-the-art approaches while lowering inference cost. We anticipate this study will drive sustainable medical AI advances, enabling real-time diagnosis, patient monitoring, and telemedicine applications in distributed healthcare. Code will be released upon acceptance.

Index Terms—Domain Incremental, Prompt Continual Learning, Medical Artificial Intelligence, Data Imbalance

I. INTRODUCTION

Modern artificial intelligence (AI) models achieve their best performance when trained on large-scale, high-quality datasets; however, in the medical domain, ethical, social, and institutional constraints make it exceedingly difficult to obtain such data [1], [2]. Variations in disease prevalence and restrictions on external data transfer render the collection of medical data and centralized training practically impossible [3]. Moreover, because medical data are captured using diverse diagnostic devices and reflect demographic differences across hospitals, distribution shifts frequently occur, leading to performance degradation in real world deployment. Indeed, a Google developed medical AI model demonstrated excellent performance during development but suffered abrupt drops in accuracy upon deployment in clinical settings [4], [5]. Consequently, there is a growing need for approaches that can overcome these practical challenges.

In this work, we focus on Continual Learning (CL), which enables models to incrementally learn from data generated independently at each hospital, taking into account the unique characteristics of medical data. CL supports retention of previously acquired knowledge while effectively incorporating new data in settings subject to domain shifts and continuously evolving environments. Given the extreme restrictions on data sharing among hospitals, updating models locally at each institution is essential. However, traditional AI training methods, when unable to access prior data, are prone to catastrophic forgetting during sequential learning [6]–[8].

When applying CL in medical settings, several factors must be considered. First, medical imaging devices are heterogeneous rather than uniform, making it critical to explicitly track inter device differences [9], [10]. Additionally, physiological variations among patients can introduce subtle color and texture differences in images that must be managed effectively. Although domain adaptation and generalization techniques can partially mitigate these issues, they remain insufficient to fully address catastrophic forgetting induced by continuous data shifts.

To address these challenges, we adopt a prompt-based continual learning (PCL) framework that prioritizes both computational efficiency and data privacy. Existing prompt-based methods often rely on multiple high-compute backbones such as Vision Transformers (ViT), or introduce additional query generation steps that impose considerable overhead [11]–[13]. Although recent efforts [14] have attempted to mitigate these limitations, they do not provide a comprehensive solution. Moreover, to the best of our knowledge, most existing prompt-based CL approaches have focused primarily on natural images. Therefore, to develop a prompt-based CL approach tailored to the medical domain, we build upon and extend the method proposed in [14]. Specifically, we introduce a unified prompt pool that merges the layer-wise prompt sets into a single shared pool. During each training stage, only a minimal subset of prompts is expanded, while the remainder are kept fixed to reduce redundancy and prevent overfitting. Additionally, we propose a novel regularization term to promote effective and stable learning. Experimental results on three public diabetic retinopathy datasets [15]–[17] demonstrate that our method significantly outperforms state-of-the-art (SOTA)

[†]Corresponding author.

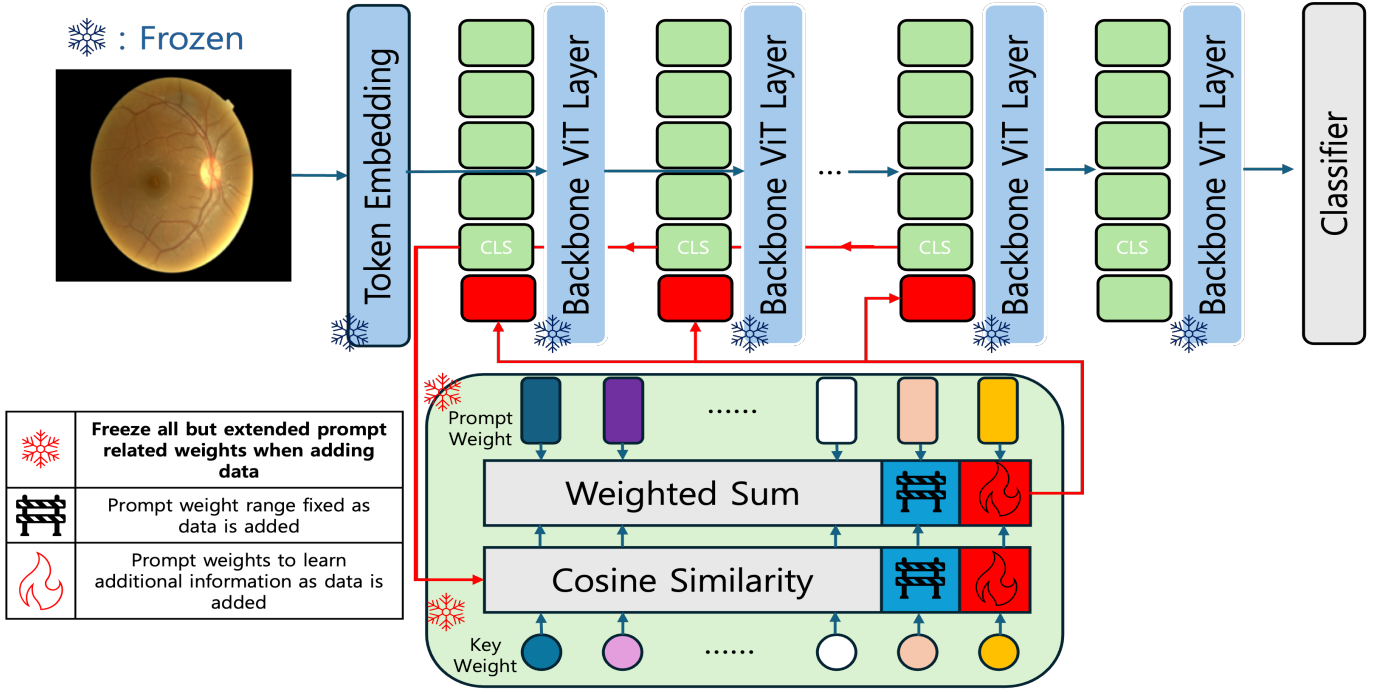


Fig. 1. This figure presents the overall architecture proposed in this study, which integrates an enhanced prompt pool. At each layer, the [CLS] token serves as a query, and the resulting layer-wise queries are centrally managed through the prompt pool integration module. This integration generates the prompts for the subsequent layer, which are then combined with x_l and propagated forward. Additionally, at each training stage, only a small number of new prompts are introduced through a minimal prompt expansion mechanism, while all previously learned prompts remain frozen.

approaches, achieving higher accuracy and F1-scores while substantially reducing computational cost.

The main contributions of this study are as follows:

- We consolidate layer wise prompt pools into a unified prompt pool and propose a new regularization term to train it effectively.
- By employing a single backbone instead of multiple models, we dramatically reduce computational cost while outperforming existing SOTA methods.
- We introduce a prompt-based continual learning strategy tailored to the medical domain that relies on expanding only a small number of prompts.

II. RELATED WORK

To position our work within the landscape of continual learning (CL), we review recent surveys [5], [18] and categorize existing methods into four main classes.

Regularization Based Methods. Regularization based approaches introduce penalty terms into the loss function to encourage the model to retain important weights from previous tasks. Examples include Elastic Weight Consolidation (EWC) [19] and Synaptic Intelligence [20], which estimate the importance of each parameter and penalize changes proportionally [21], [22]. While effective on low dimensional or simple datasets, these methods struggle when data complexity and dimensionality increase, as the approximation of parameter importance becomes unreliable.

Architecture Based Methods. Architecture based strategies dynamically adapt the network structure to accommodate new

tasks. Techniques such as Progressive Neural Networks and Supermasks allocate new subnetworks or masks per task, offering strong scalability [23], [24]. However, they incur growing memory and computation costs with each new task, making them less practical for long sequences of tasks or resource constrained environments.

Rehearsal Based Methods. Rehearsal based approaches store a small buffer of past examples and replay them alongside new data to prevent forgetting. Methods like iCaRL [25] and Dark Experience Replay [26] have demonstrated strong performance on image benchmarks [27], [28]. Yet, the need to store real data raises serious privacy and storage concerns particularly acute in the medical domain, where data sharing is heavily restricted.

Prompt-Based Methods. Prompt-based continual learning fixes the majority of the pretrained model's parameters and learns only a small set of prompt vectors for each task. This design preserves existing knowledge while adapting efficiently to new domains, drastically reducing both memory and computation overhead [11], [12], [14]. These methods have shown promise on natural-image benchmarks but have not yet been widely explored for medical data.

The Need for Medical Domain PCL. In summary, while regularization, architecture, and rehearsal methods each bring valuable insights, their applicability in the medical domain is limited by data complexity, resource constraints, and privacy issues. Prompt-based methods offer an appealing alternative by leveraging a fixed backbone and learning lightweight prompts.

In this work, we extend the prompt-based paradigm to medical imaging, investigating its feasibility across distributed hospital datasets.

III. PRELIMINARY

The primary objective of this paper is to efficiently mitigate domain shift arising from multiple hospitals and various sources, and to comprehensively address the drawback of existing prompt-based CL methods that require multiple backbones during training and inference. As noted earlier, we adopt a prompt-based CL approach to solve these issues. Our core methodology is based on the recent One-Stage Prompt-based Continual Learning framework [14]; all unspecified settings follow those in the referenced work.

A. Continual Learning Problem Setting

In this section, we briefly describe the continual learning (CL) environment. We consider a scenario in which data collected at each hospital are learned via CL. To this end, we utilize publicly available datasets collected from different hospitals with identical disease and severity labels [15]–[17]. During training, our CL environment sequentially and independently learns from data with dynamic distributions at each stage, meaning that samples from previous stages or future data are inaccessible. We also assume no rehearsal buffer is used, following the rehearsal-free CL paradigm defined in [18]. Furthermore, our experiments are conducted under a domain-incremental learning (DIL) setting where task identities are unknown. For a detailed explanation of task identity, we refer to [18] due to space limitations. The training data are denoted as $D = \{D_1, D_2, \dots, D_n\}$, for $D_n = \{X_{n,b}, Y_{n,b}\}$. Where, n indicates the stage index of arriving datasets, $X_{n,b}$ represents an input image, and $Y_{n,b}$ the corresponding ground-truth label in an image recognition task.

B. OS-Prompt

To understand this paper, it is necessary to review the foundational OS-Prompt and the limitations of existing prompt-based continual learning (PCL) methods. Conventional PCL approaches sometimes incur high computational costs by requiring an additional query function (e.g., a Vision Transformer) to generate prompt queries [14]. To address this issue, OS-Prompt was proposed. OS-Prompt removes the query function and directly uses the [CLS] token embedding extracted from the intermediate layer l of the backbone as the query (q_l), as follows. The [CLS] token is a learnable embedding prepended to the patch embedding sequence in Vision Transformer (ViT), designed to aggregate global contextual information across the entire image. As it passes through multiple self-attention layers, the [CLS] token captures a holistic representation of the input, making it suitable for use as a query in prompt selection. Furthermore, the corresponding formulation can be represented as follows:

$$q_l = x_l[\text{CLS}], \quad q_l \in \mathbb{R}^{1 \times D} \quad (1)$$

Here, $x_l \in \mathbb{R}^{N \times D}$ denotes the input token embeddings at layer l , where N is the number of input tokens and D is the embedding dimension. To select prompts from the existing prompt pool, a cosine similarity based weighted sum is used. The prompt key matrix K_l is formed by stacking the L_p prompt key vectors $[k_l^1, k_l^2, \dots, k_l^{L_p}]$ and transposing, yielding a matrix in $\mathbb{R}^{L_p \times D}$. Here, L_p is the total number of prompts, k_l^m is the key vector of the m -th prompt ($k_l^m \in \mathbb{R}^{1 \times D}$), and the corresponding prompt value vector is $p_l^m \in \mathbb{R}^{1 \times D}$. Using the cosine similarity function $\gamma(\cdot)$, the selected prompt is computed as follows.

$$\phi_l = \sum_{m=1}^{L_p} \gamma(q_l, k_l^m) p_l^m, \quad \phi_l \in \mathbb{R}^{1 \times D} \quad (2)$$

C. OS-Prompt++

OS-Prompt removes the query function to reduce computational cost, but relying solely on the [CLS] token from an intermediate layer limits representational capacity and yields only marginal performance gains. OS-Prompt++ [14] addresses this by reintroducing the query function during training to enrich the [CLS] token's expressiveness.

First, the final-layer [CLS] token r is extracted via the original query function:

$$r = R(x), \quad r \in \mathbb{R}^{1 \times D}. \quad (3)$$

Next, we compute the normalized cosine similarities between r (or the intermediate-layer query q_l) and each prompt key in K_l . Although the structure is the same for both r and q_l , the input differs:

$$A_l = \text{Softmax}\left(\frac{K_l r^\top}{\|K_l\|_2 \|r\|_2}\right), \quad A_l \in \mathbb{R}^{L_p \times 1}. \quad (4)$$

These similarity weights are then used to reweight and aggregate prompt values, supplementing the limited representation:

$$p_l(r) = \sum_{m=1}^{L_p} A_l^m p_l^m. \quad (5)$$

As these results show, there remains room for improvement toward a truly single-backbone solution. Addressing this limitation is a primary goal of our work. While OS-Prompt variants can also leverage prefix-tuning to enhance layer-wise attention, we do not adopt prefix-tuning in the present study.

IV. PROPOSED METHOD

Primarily, our goal is to achieve superior continual-learning performance using a single backbone. To this end, our methodology comprises three key components: (1) integration of a prompt pool, (2) minimal prompt expansion, and (3) the addition of a consistency-enforcing regularization term.

As shown in Table I, medical datasets often exhibit severe long-tailed class distributions, which exacerbate catastrophic forgetting as training stages progress. To address this, we adopt the powerful Dino-v2 backbone [29]. Although larger Dino-v2 variants generally yield better accuracy, Table IX reveals that

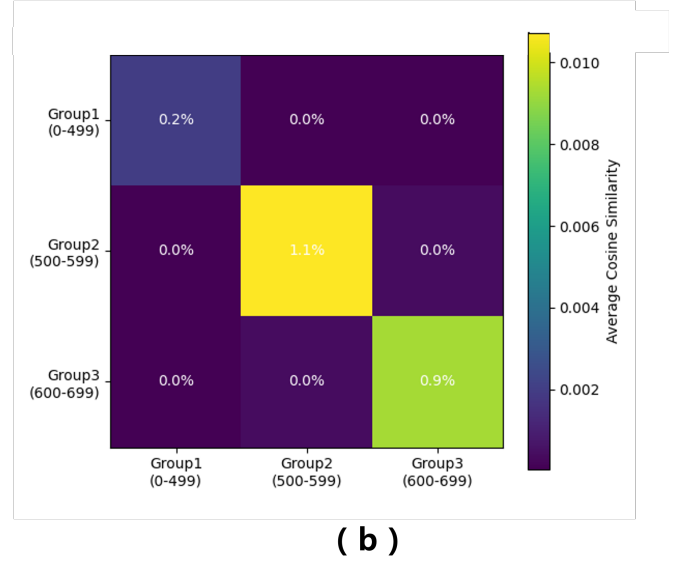
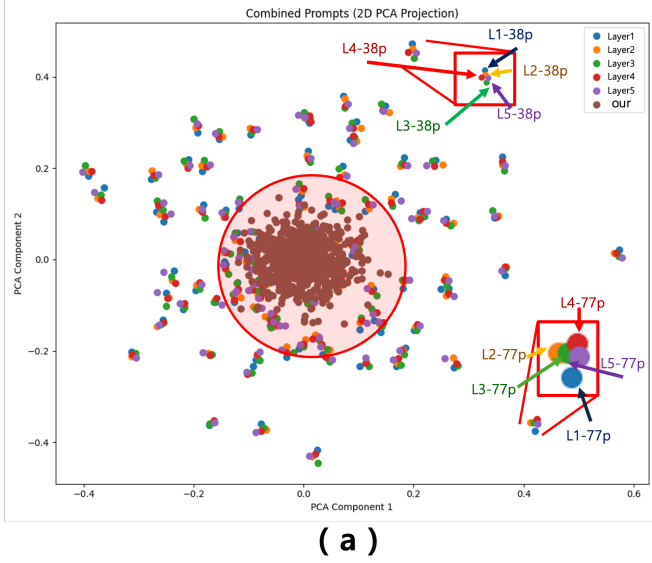


Fig. 2. (a) visualizes the prompts of OS-Prompt (independent pool) and our proposed approach (integrated pool). The dots corresponding to layers 1 through 5 represent the prompts from OS-Prompt, while the brown dots (Ours) indicate the prompts generated by our integrated pool. Refer to the upper-right corner of the figure for further details. (b) shows that, as training stages progress, the newly added prompts do not learn redundant or overlapping information, suggesting that each prompt captures distinct features.

their parameter counts grow dramatically. Hence, we selected **facebook/dinov2-base (86.6 M parameters)** for its balanced trade-off between representational capacity and computational efficiency.

Our experiments demonstrate that this strong backbone, combined with our prompt-based design and regularization, effectively mitigates both data imbalance and catastrophic forgetting in medical continual-learning scenarios. The overall architecture of our approach is illustrated in Figure 1.

A. Motivation for Proposal and Integration of Prompt-Pool

In this section, we explain the motivation behind integrating the prompt pool and describe our proposed Integration of Prompt-Pool. Based on [19, 41], We hypothesized that, since medical images are acquired according to standardized protocols, prompts in PCL should be fine-tuned to capture highly similar information for optimal performance. To test this, we visualized the prompts. Figure 2.a shows this visualization: the brown dots in the top right correspond to prompts included in our Integration of Prompt-Pool, while the other colors represent prompts from each layer of OS-Prompt++. From this, we observed that although existing PCL methods learn similar information across layers, they do not achieve the expected fine-grained adjustment. Therefore, we enhance the prompt pool to enable such fine-tuning. Specifically, we integrate all layer-wise prompt pools to fully exploit inter-layer similarities, guiding the model to learn subtle distinctions as detailed in Section 4.2.

Having presented the motivation, we now detail the structure of the Integration of Prompt-Pool. As in Equation (1), we use each layer’s [CLS] token embedding as the prompt query

q_l . Our prompt keys become $k^m \in \mathbb{R}^{1 \times D}$ and prompt value vectors $p^m \in \mathbb{R}^{1 \times D}$. Consequently, the prompt computation is modified as follows:

$$\phi_l = \sum_{m=1}^{L_p} \gamma(q_l, k^m) p^m, \quad \phi_l \in \mathbb{R}^{1 \times D}. \quad (6)$$

The resulting prompt ϕ_l is then integrated into the layer transformation:

$$x_{l+1} = f_l(x_l, \phi_l). \quad (7)$$

B. Few Prompt Expansion

In this subsection, we introduce the Few Prompt Expansion strategy, which leverages existing prompt information to its fullest while learning the fine grained features necessary for domain expansion. First, we freeze all prompts in the integrated prompt pool as described in Section 4.1. Next, we expand the prompt set by 20% of the original L_p prompts, a heuristic choice that remains fixed throughout task progression. However, newly added prompts may initially have less influence compared to well-trained prompts, potentially limiting their effectiveness in learning. To address this, we introduce the following formulation to ensure the added prompts more effectively capture new information.

We first modify Equation (4) to:

$$z_l = \text{Softmax}\left(\frac{K_l p_*^\top}{\|K_l\|_2 \|p_*\|_2}\right), \quad z_l \in \mathbb{R}^{M \times 1}, \quad (8)$$

where p_* denotes the normalized prompt vector. We then refine this to:

$$S_{b,m} = 1 - (z_l)^\top, \quad L_s = \frac{1}{b \times L_p} \sum_{m=1}^{L_p} S_{b,m}, \quad (9)$$

where b is the batch size and L_p the total number of prompts.

Finally, the overall loss function used for training is:

$$L_{\text{total}} = L_{\text{CE}} + \lambda L_s, \quad (10)$$

where λ is a hyperparameter set to 0.001 in this study to control the strength of the regularization term.

TABLE I
DISTRIBUTION OF DATASETS USED FOR TRAINING

Dataset	Normal (0)	Mild (1)	Severe (2)
Aptos 2019 [15]	1805	1562	295
DDR [16]	6266	5343	913
Diabetic [17]	5000	8608	708

V. EXPERIMENTS

A. Experiment Settings

In this section, we describe our experimental setup in detail to substantiate our claims. First, we introduce the datasets used in our experiments; second, we outline the data augmentation and preprocessing methods, baseline validation procedures, evaluation metrics, and implementation environment. Detailed information about the datasets can be found in Table I, and the experimental settings are provided in Table II.

Dataset. We simulate a domain-incremental scenario using three publicly available datasets collected from different hospitals with identical disease and severity labels: Aptos2019 [15], LI2019 (DDR) [16], and Diabetic Retinopathy Detection (Dia) [17]. Prior to training, and following the procedure in [30], each dataset’s original classes are consolidated into three joint labels. The datasets are then presented to the model in the sequence:

$$\text{Aptos2019} \rightarrow \text{DDR} \rightarrow \text{Dia}.$$

Experimental Details. During training, data augmentations including HorizontalFlip, Rotation, and VerticalFlip are applied at random. ViT preprocessing is performed using the AutoImageProcessor (weights: facebook/dinov2-base) from the transformers library; see Table II for detailed settings. Baseline methods are validated using the rigorously implemented CL library from [26], [31], with any additional required code custom implemented.

Standard PCL approaches are often evaluated on large-scale datasets such as ImageNet or CIFAR-100. Consequently, prior studies measure overall catastrophic forgetting using metrics such as Backward Transfer (BWT), Final Average Accuracy (FAA), Average Accuracy (AvgACC), and Average Forgetting (AvgF). However, since our experiments use limited-size medical datasets, we directly observe performance changes at each PCL stage and additionally report accuracy and F1-score to account for class imbalance. All experiments were implemented in Python and PyTorch (version 2.4.1+cu118).

TABLE II
EXPERIMENT SETTINGS

Item	Value
GPU	$2 \times \text{V100}$
RAM	256GB
Learning Rate	1×10^{-4}
Scheduler	Cosine Scheduler
Number of Prompts (L_p)	500
Prompt Dimension (D)	768
Optimizer	AdamW
Early Stop Patience	5
Epochs	100
Batch Size	64
Image Size	224×224

B. Experimental Results

In this session, to aid the readers’ understanding, we separate the results of each table and figure into individual sections and discuss them in detail.

Stage-Wise Prompt Independence and Fine-Grained Feature Encoding. As discussed in Section 4, we hypothesize that the prompts added at each stage should not only retain previously acquired information but also capture new, fine-grained features. Figure 2.(b) supports this hypothesis by presenting a similarity matrix of the prompts introduced at successive stages under our proposed method. The clear diagonal pattern indicates that prompts are learned independently at each stage, with minimal redundancy across stages. In other words, newly added prompts effectively encode novel information without overlapping with existing ones. Additionally, Figure 2.(a) demonstrates that the expanded prompts focus on subtle distinctions. In this figure, the brown markers denote prompts from the integrated prompt pool, initially learned via the base OS-Prompt model, while the other markers represent stage-specific prompts. Whereas the prompts from OS-Prompt broadly span the feature space, our integrated prompts form tighter clusters that reflect more refined feature representations. Finally, the quantitative results in Table III indicate that our method outperforms existing state-of-the-art (SOTA) models, providing empirical evidence for the hypothesis presented in Section 4.1.

Comparative Performance Analysis with SOTA PCL Methods. In this subsection, we describe the performance comparison results presented in Table III. Table III compares existing state-of-the-art PCL methods with our proposed approach in terms of accuracy and F1-Score on each dataset at the final stage. Overall, our method achieves higher accuracy and F1-Score compared to existing techniques, demonstrating superior performance in continual learning for the medical domain. This improvement is closely related to the prompt distributions shown in Figure 2.a. Existing SOTA PCL methods are primarily designed for natural images and require a wide range of prompts to accommodate various capture angles and compositional changes. In contrast, medical imaging follows strictly defined protocols with consistent framing and conditions, making it essential to track subtle variations in color

TABLE III
FINAL ACCURACY (ACC) AND F1-SCORE (F1) RESULTS AFTER THE FINAL STAGE AND PERFORMANCE COMPARISON WITH OTHER PROMPT-BASED CL MODELS. (RED BOLD INDICATES THE HIGHEST PERFORMANCE; SCORES ARE MEAN VALUES WITH NEGLIGIBLE DEVIATIONS.)

Ref	Model	Aptos 2019		DDR		Dia	
		Acc	F1	Acc	F1	Acc	F1
ECCV2024	OS [14]	0.687	0.637	0.693	0.648	0.619	0.568
ECCV2024	OS++ [14]	0.743	0.686	0.697	0.655	0.623	0.565
CVPR2023	Coda-Prompt [12]	0.682	0.646	0.721	0.697	0.663	0.557
CVPR2022	L2P [11]	0.353	0.174	0.421	0.194	0.603	0.252
ECCV2022	Dual-prompt [32]	0.363	0.185	0.435	0.222	0.604	0.259
Ours	Ours	0.845	0.758	0.789	0.742	0.690	0.650

profiles across devices and patient specific characteristics. Consequently, while prompt clusters in the natural domain are broadly distributed, more granular prompt distributions prove effective in the medical domain. Our results suggest that these domain specific characteristics underlie the performance limitations of existing SOTA PCL methods and highlight the need for customized learning strategies tailored to each domain.

Stage-Wise Forgetting Mitigation and Performance Gains. In this subsection, we explain the performance comparison results presented in Table IV. As discussed in Section 5.2, Table IV shows how accuracy and F1-score evolve across the training stages. We use OS-Prompt++, which achieved the best results in Table III, as our baseline. The most notable result is that our method not only mitigates catastrophic forgetting but also delivers higher overall performance. Remarkably, while OS-Prompt++ relies on two ViT backbones (Double ViT), our approach uses only a single ViT and still outperforms it. Furthermore, because we employ only one ViT even with expanded prompts our method requires substantially lower FLOPs, demonstrating its efficiency.

VI. ABLATION STUDY

In this session, we conduct ablation studies to enhance the interpretability and reliability of our research by elucidating clear causal relationships underlying performance improvements. Ultimately, the goal of this session is to identify directions for model enhancement and to explicitly highlight the key contributing components. Lastly, the integration of the prompt pool was discussed in detail in Session 6.

For clarity, we summarize the key points of each session below:

- **Session 6.1:** We demonstrate the necessity of integrating a strong backbone into prompt-based continual learning (PCL) and show that the superior performance of our method cannot be attributed to the backbone alone.
- **Session 6.2:** To rigorously validate the findings of Session 6.1, we introduce additional metrics Final Average Accuracy (FAA, Equation. 12), Backward Transfer (BWT, Equation 13), and Average Forgetting (AvgF, Equation. 14) thereby reinforcing our claims.
- **Session 6.3:** We evaluate the performance impact of the loss function proposed in Section 4.2, demonstrating that the proposed loss yields a significant improvement.

- **Session 6.4:** We analyze performance variations under different prompt expansion ratios as CL progresses. From this analysis, we select an optimal expansion ratio and identify that indiscriminate prompt expansion does not contribute to performance gains.

A. Effectiveness of Strong Backbones in Prompt-Based Continual Learning.

In Table V, we demonstrate both the necessity of incorporating a powerful backbone into prompt-based continual learning (PCL) and that our method’s superior performance cannot be attributed to the backbone alone. We examine foundation models such as Dino-V2 because, unlike conventional backbones, these models are pretrained on massive datasets and are capable of extracting high-quality features across diverse tasks. Although several prior studies have utilized foundation models to achieve outstanding few-shot and zero-shot performance [33]–[37], their applicability within the PCL domain remains underexplored.

Given the severe class imbalance and limited sample sizes commonly observed in the medical domain, we anticipated greater performance gains from adopting a foundation model. Accordingly, we selected OS-Prompt++, which recorded the highest performance in Table III, as our baseline and compared the following three configurations:

- Original OS-Prompt++ (without backbone enhancement),
- OS-Prompt++ with a Dino-V2 backbone,
- Our proposed method.

To ensure a fair comparison, all experimental conditions were held constant except for the backbone. Comparing the original OS-Prompt++ with its Dino-V2 variant, we observe that the incorporation of Dino-V2 improves both overall accuracy and robustness against forgetting. This result indicates that a stronger backbone provides generalization benefits analogous to few-shot and zero-shot learning, even within PCL settings. Importantly, our full method still outperforms both variants, demonstrating that the gains achieved by Few Prompt Expansion and Integration of the Prompt Pool extend beyond what can be attributed to backbone strength alone. Additional experiments and metrics are presented in Section 6.2 (Table VI) for further analysis.

TABLE IV

TRACKING AND COMPARING VARIOUS CATASTROPHIC FORGETTING OUTCOMES DURING STAGE PROGRESSION (WHERE **Red** INDICATES DATA LEARNED AT THE CURRENT STEP, **Blue** INDICATES PREVIOUSLY LEARNED DATA (SEEN), AND **Black** INDICATES UNSEEN DATA) [ACCURACY (ACC), F1-SCORE (F1), OS PROMPT++ (OS++)]; **HORIZONTAL: TRAINING DATA, VERTICAL: EVALUATION DATA**. ADDITIONALLY, THE FLOPS ROW INDICATES THE AMOUNT OF COMPUTING RESOURCES USED.

Train	Dataset	Evaluation											
		OS-Prompt++ (Double Backbone)						Ours (Single Backbone)					
		Aptos 2019		DDR		Dia		Aptos 2019		DDR		Dia	
		Acc	F1	Acc	F1	Acc	F1	Acc	F1	Acc	F1	Acc	F1
Stage 1	Aptos 2019	0.868	0.753	0.565	0.474	0.409	0.354	0.901	0.767	0.601	0.447	0.453	0.381
Stage 2	DDR	0.707	0.638	0.797	0.748	0.508	0.413	0.866	0.663	0.878	0.844	0.636	0.534
Stage 3	Dia	0.743	0.686	0.697	0.655	0.623	0.565	0.849	0.761	0.772	0.723	0.701	0.656
FLOPs		66.42 GFLOPs						44.17 GFLOPs					

B. Quantitative Validation Using FAA, BWT, and AvgF Metrics.

In this subsection, we discuss the results in Table VI, which rigorously validate the performance of the experiments from Table V using standard continual learning metrics. The detailed formulas for these metrics are given below:

As shown in Table VI, introducing a powerful backbone yields improvements in all metrics Average Accuracy(AvgACC) (Equation. 11), Final Average Accuracy(FAA) (Equation. 12), Backward Transfer(BWT) (Equation. 13), and Average Forgetting(AvgF) (Equation. 14). Nevertheless, our proposed method still outperforms the backbone-enhanced variant, confirming that the additional gains stem from our Few Prompt Expansion and Integration of Prompt-Pool techniques. The best results in Table VI are highlighted in **bold red**.

Notation:

- **T**: Total number of tasks (or stages).
- **A_{i,j}**: Accuracy after training on task *i* and testing on task *j*.
- **AvgACC**: Average Accuracy,

$$\text{AvgACC} = \frac{1}{T} \sum_{i=1}^T A_{i,i} \quad (11)$$

the mean of the diagonal entries $A_{i,i}$.

- **FAA**: Final Average Accuracy,

$$\text{FAA} = \frac{1}{T} \sum_{i=1}^T A_{T,i} \quad (12)$$

the mean of the last-row entries $A_{T,i}$.

- **BWT**: Backward Transfer,

$$\text{BWT} = \frac{1}{T-1} \sum_{i=2}^T \sum_{j=1}^{i-1} (A_{j,i} - A_{i,i}) \quad (13)$$

the average change in performance on previous tasks.

- **AvgF**: Average Forgetting,

$$\text{AvgF} = \frac{1}{T-1} \sum_{i=1}^{T-1} \left(\max_{1 \leq k \leq T-1} A_{k,i} - A_{T,i} \right) \quad (14)$$

the mean drop from the best past accuracy to the final accuracy for each task.

TABLE V

WE COMPARE THE RESULTS OF FATAL FORGETTING DURING THE STEPWISE PROGRESSION OF THE BASELINE MODEL, THE INTRODUCTION OF A STRONGER BACKBONE, AND THE METHODOLOGY OF THIS STUDY. THROUGH THESE EXCLUSION STUDIES, WE HIGHLIGHT THE IMPORTANCE OF A GOOD BACKBONE IN PCL AND SHOW THAT THERE IS ROOM FOR FURTHER IMPROVEMENT. IT CAN BE INTERPRETED IN THE SAME WAY AS TABLE IV.

OS-Prompt++ (Original)						
Target	Aptos 2019		DDR		Diabetic	
	Acc	F1	Acc	F1	Acc	F1
Aptos 2019	0.868	0.753	0.565	0.474	0.409	0.354
DDR	0.707	0.638	0.797	0.748	0.508	0.413
Diabetic	0.743	0.686	0.697	0.655	0.623	0.565
OS-Prompt++ (Add Dino-v2)						
Target	Aptos 2019		DDR		Diabetic	
	Acc	F1	Acc	F1	Acc	F1
Aptos 2019	0.918	0.823	0.608	0.520	0.492	0.467
DDR	0.732	0.604	0.849	0.828	0.625	0.563
Diabetic	0.754	0.690	0.763	0.721	0.668	0.585
Ours						
Target	Aptos 2019		DDR		Diabetic	
	Acc	F1	Acc	F1	Acc	F1
Aptos 2019	0.901	0.767	0.601	0.447	0.453	0.381
DDR	0.866	0.663	0.878	0.844	0.636	0.534
Diabetic	0.849	0.761	0.772	0.723	0.701	0.656

C. Ablation Study on the Proposed Loss Function

In this subsection, we evaluate the performance impact of the loss proposed in Section 4.2. The results are presented in Table VII, with each metric measured after the final training stage. The detailed hyperparameter settings follow those listed in Table II. Overall, we observe consistent performance improvements. For the Dia dataset, there is a slight decrease in performance; however, this reduction is minimal compared

TABLE VI

TABLE V PERFORMANCE EVALUATION OF AVERAGE ACCURACY (AVGACC), FINAL AVERAGE ACCURACY (FAA), BACKWARD TRANSFER (BWT) AND AVERAGE FORGETTING (AVGF) ACCORDING TO EXPERIMENTS. THE BEST RESULTS IN TABLE VI ARE HIGHLIGHTED IN **BOLD RED**.

Method	AvgACC \uparrow	FAA \uparrow	BWT \uparrow	AvgF \downarrow
OS-Prompt++ (Original)	0.769	0.688	-0.113	0.113
OS-Prompt++ (Add Dino-v2)	0.812	0.728	-0.125	0.125
Ours	0.844	0.759	-0.079	0.079

to the substantial gains seen on the other datasets. Across all evaluated metrics, our method demonstrates robust performance and behaves as intended. Therefore, we consider the loss formulation introduced in Section 4.2 to be both effective and meaningful, while recognizing that further refinement is possible.

TABLE VII

PERFORMANCE COMPARISON ACCORDING TO THE USE OF LOSS(EQUATION. 10) PROPOSED IN THIS PAPER. AFTER THE FINAL STEP, THE FINAL ACCURACY (ACC) AND F1-SCORE(F-1) RESULTS ARE SHOWN.

Loss	Aptos 2019		DDR		Dia	
	Acc	F1	Acc	F1	Acc	F1
X	0.797	0.715	0.773	0.733	0.692	0.657
O	0.845	0.758	0.789	0.742	0.691	0.650

D. Impact of Prompt Expansion Ratio on Continual Learning Performance

In this subsection, we discuss the procedure for selecting the prompt expansion ratio. We evaluated candidate ratios of 10%, 20%, and 30%, and the results are presented in Table VIII. All experiments adhered to the detailed hyperparameter settings outlined in Table II. We ultimately selected a 20% expansion ratio because increasing from 10% to 20% yielded clear performance improvements, whereas further expanding to 30% increased the parameter count without corresponding gains and even caused slight performance degradation. These findings indicate that indiscriminate expansion of parameters does not guarantee better performance. Additionally, in Section 7(Future Works), we discuss further strategies that could be introduced to enhance performance.

VII. CONCLUSION AND FUTURE WORK

In this paper, we presented a novel approach for prompt-based continual learning (PCL) tailored to the medical domain by integrating a powerful foundation model backbone and introducing an efficient prompt management strategy. Our findings reveal several key insights that contribute to both the theoretical understanding and practical advancement of PCL.

First, we demonstrated that incorporating a strong backbone, such as Dino-V2 pretrained on large-scale datasets, significantly improves PCL performance. As a foundation

model pretrained on large-scale datasets, Dino-V2 produces generalizable and semantically rich representations, which play a crucial role in mitigating catastrophic forgetting in continual learning. Through experiments on three public diabetic retinopathy datasets (Aptos2019 [15], DDR [16], Dia [30].), we observed consistent performance improvements, including at least a 10% increase in classification accuracy and a 9-point gain in F1-score. These results underscore the importance of leveraging foundation models for enhancing robustness and generalization in continual learning scenarios.

Second, we highlighted the necessity of domain-specific considerations in designing continual learning systems for medical applications. Whereas natural image datasets used in prior PCL studies often lack consistency in acquisition protocols, medical imaging data is captured under strict clinical standards. This difference has a profound impact on the behavior of continual learning algorithms. Our experiments in Section 6 demonstrate that PCL strategies optimized for natural images do not generalize well to medical datasets, and that our method offers a substantial performance advantage in the medical setting.

Third, we introduced an efficient prompt expansion mechanism that selectively adds a small number of prompts at each stage rather than expanding the prompt pool indiscriminately. Combined with an integrated prompt pool, this design enables the model to capture fine-grained task-specific features while preserving previously acquired knowledge. This strategy reduces memory and computational costs while maintaining competitive accuracy and stability, as evidenced by the prompt similarity visualizations in Figure 2 and the quantitative results in Table III.

Future Works. Despite these contributions several limitations remain. **First**, our evaluation was conducted on a limited number of datasets focused on diabetic retinopathy classification. Although these datasets are diverse, they represent a single disease context. To ensure broader applicability, we plan to extend our experiments to include other imaging modalities such as CT, MRI, and pathology, as well as different task types including segmentation and detection.

Second, the hyperparameters in our framework, such as the prompt expansion ratio and loss weights, were chosen based on heuristic methods. While they yielded strong empirical results, a more systematic exploration of the hyperparameter space using automated optimization techniques may further improve performance. We intend to conduct comprehensive ablation studies and release findings through an open source repository.

Third, our current method adopts a fixed-stage prompt expansion schedule, adding a predefined number of prompts at each stage regardless of task complexity. However, in real world scenarios, task difficulty may vary across stages. We aim to explore adaptive prompt expansion strategies that dynamically adjust the number of prompts based on data complexity, model confidence, or validation performance, potentially leveraging reinforcement learning or meta-learning approaches.

Fourth, while this study employs Dino-V2 as the backbone,

TABLE VIII
PERFORMANCE EVALUATION BY PROMPT EXPANSION RATIO

# Prompt Extensions	Stage (Train Dataset)	Aptos 2019		DDR		Dia	
		Acc	F1	Acc	F1	Acc	F1
50 (10%)	Stage 1 (Aptos 2019)	0.898	0.765	0.592	0.440	0.446	0.372
	Stage 2 (DDR)	0.830	0.659	0.868	0.852	0.630	0.534
	Stage 3 (Dia)	0.803	0.751	0.739	0.706	0.692	0.659
100 (20%)	Stage 1 (Aptos 2019)	0.901	0.767	0.601	0.447	0.453	0.381
	Stage 2 (DDR)	0.866	0.663	0.878	0.844	0.636	0.534
	Stage 3 (Dia)	0.849	0.761	0.772	0.723	0.701	0.656
150 (30%)	Stage 1 (Aptos 2019)	0.901	0.774	0.608	0.469	0.470	0.408
	Stage 2 (DDR)	0.816	0.668	0.869	0.856	0.637	0.543
	Stage 3 (Dia)	0.836	0.757	0.757	0.709	0.694	0.636

we did not experiment with ViT models specifically designed for the medical domain, such as Med-CLIP [38] or Med-ViT [39]. These models may offer better performance and efficiency in medical tasks. Therefore, we plan to benchmark a broader set of backbone architectures to identify the most suitable option for continual learning in medical applications.

Finally, to promote open science and reproducibility, we will release our codebase, pretrained models, and processed datasets upon acceptance of this paper. The repository will be continuously maintained and updated to support further development in the field.

In conclusion, our study demonstrates that combining powerful backbones with efficient prompt management provides a robust solution to the challenges of continual learning in the medical domain. We believe that our insights will guide future research and facilitate the development of practical, generalizable, and domain-aware continual learning systems for clinical environments and beyond.

APPENDIX

A. Parameter counts for dinov2 models

This table IX summarizes the four variants of the facebook/dinov2 family, ordered by increasing model size and corresponding parameter counts. Here, **M** denotes million parameters and **B** denotes billion parameters. Using the Hugging Face library, we loaded and employed the aforementioned model.

TABLE IX
PARAMETER COUNTS FOR FACEBOOK/DINO2 MODELS

Model	Parameters
facebook/dinov2-small	22.1 M
facebook/dinov2-base	86.6 M
facebook/dinov2-large	304 M
facebook/dinov2-giant	1.14 B

B. Example Calculation for Table VI Metrics.

Prior to submission, peer reviewers noted that readers might find Table VI confusing. To clarify, we provide a concise example of how the “Ours” row is computed, using minimal notation due to space constraints. The calculations for AvgACC

(Average Accuracy), FAA (Final Average Accuracy), BWT (Backward Transfer), and AvgF (Average Forgetting) are given below.

The matrix A records the accuracy $A_{i,j}$ on task j immediately after completing stage i (tasks: 1 = Aptos2019, 2 = DDR, 3 = Dia).

$$A = \begin{bmatrix} A_{1,1} & A_{1,2} & A_{1,3} \\ A_{2,1} & A_{2,2} & A_{2,3} \\ A_{3,1} & A_{3,2} & A_{3,3} \end{bmatrix}, \quad A_{i,j} = \begin{cases} 0.901 & (i,j) = (1,1) \\ 0.601 & (1,2) \\ 0.453 & (1,3) \\ 0.866 & (2,1) \\ 0.878 & (2,2) \\ 0.636 & (2,3) \\ 0.849 & (3,1) \\ 0.772 & (3,2) \\ 0.701 & (3,3) \end{cases}$$

$$m_1 = A_{1,1}, \quad m_2 = \frac{A_{2,1} + A_{2,2}}{2}, \quad m_3 = \frac{A_{3,1} + A_{3,2} + A_{3,3}}{3}.$$

$$\text{AvgACC} = \frac{m_1 + m_2 + m_3}{3},$$

$$\text{FAA} = \frac{A_{3,1} + A_{3,2} + A_{3,3}}{3},$$

$$\text{BWT} = \frac{(A_{3,1} - A_{1,1}) + (A_{3,2} - A_{2,2})}{2},$$

$$\text{AvgF} = \frac{(\max\{A_{1,1}, A_{2,1}\} - A_{3,1}) + (\max\{A_{1,2}, A_{2,2}\} - A_{3,2})}{2}.$$

REFERENCES

- [1] S. Gerke, T. Minssen, and G. Cohen, “Ethical and legal challenges of artificial intelligence-driven healthcare,” in *Artificial intelligence in healthcare*. Elsevier, 2020, pp. 295–336.
- [2] J. Herington, M. D. McCradden, K. Creel, R. Boellaard, E. C. Jones, A. K. Jha, A. Rahmim, P. J. Scott, J. J. Sunderland, R. L. Wahl *et al.*, “Ethical considerations for artificial intelligence in medical imaging: data collection, development, and evaluation,” *Journal of Nuclear Medicine*, vol. 64, no. 12, pp. 1848–1854, 2023.
- [3] C. Tschider, M. C. Compagnucci, and T. Minssen, “The new eu–us data protection framework’s implications for healthcare,” *Journal of Law and the Biosciences*, vol. 11, no. 2, p. lsae022, 09 2024. [Online]. Available: <https://doi.org/10.1093/jlb/lsae022>

- [4] E. Beede, E. Baylor, F. Hersch, A. Iurchenko, L. Wilcox, P. Ruamvi-boonsuk, and L. M. Vardoulakis, "A human-centered evaluation of a deep learning system deployed in clinics for the detection of diabetic retinopathy," in *Proceedings of the 2020 CHI conference on human factors in computing systems*, 2020, pp. 1–12.
- [5] M. A. Qazi, A. U. R. Hashmi, S. Sanjeev, I. Almakky, N. Saeed, C. Gonzalez, and M. Yaqub, "Continual learning in medical imaging: A survey and practical analysis," *arXiv preprint arXiv:2405.13482*, 2024.
- [6] M. Abdelsalam, M. Faramarzi, S. Sodhani, and S. Chandar, "Iirc: Incremental implicitly-refined classification," in *Proceedings of the IEEE/CVF Conference on Computer Vision and Pattern Recognition (CVPR)*, June 2021, pp. 11 038–11 047.
- [7] A. Agarwal, B. Banerjee, F. Cuzzolin, and S. Chaudhuri, "Semantics-driven generative replay for few-shot class incremental learning," in *Proceedings of the 30th ACM international conference on multimedia*, 2022, pp. 5246–5254.
- [8] E. Belouadah and A. Popescu, "Scail: Classifier weights scaling for class incremental learning," in *Proceedings of the IEEE/CVF Winter Conference on Applications of Computer Vision (WACV)*, March 2020.
- [9] H. Guan and M. Liu, "Domain adaptation for medical image analysis: a survey," *IEEE Transactions on Biomedical Engineering*, vol. 69, no. 3, pp. 1173–1185, 2021.
- [10] R. Kushol, A. H. Wilman, S. Kalra, and Y.-H. Yang, "Dsmri: domain shift analyzer for multi-center mri datasets," *Diagnostics*, vol. 13, no. 18, p. 2947, 2023.
- [11] Z. Wang, Z. Zhang, C.-Y. Lee, H. Zhang, R. Sun, X. Ren, G. Su, V. Perot, J. Dy, and T. Pfister, "Learning to prompt for continual learning," in *Proceedings of the IEEE/CVF conference on computer vision and pattern recognition*, 2022, pp. 139–149.
- [12] J. S. Smith, L. Karlinsky, V. Gutta, P. Cascante-Bonilla, D. Kim, A. Arbelle, R. Panda, R. Feris, and Z. Kira, "Coda-prompt: Continual decomposed attention-based prompting for rehearsal-free continual learning," in *Proceedings of the IEEE/CVF Conference on Computer Vision and Pattern Recognition*, 2023, pp. 11 909–11 919.
- [13] M. Menabue, E. Frascaroli, M. Boschini, E. Sangineto, L. Bonicelli, A. Porrello, and S. Calderara, "Semantic residual prompts for continual learning," in *European Conference on Computer Vision*. Springer, 2024, pp. 1–18.
- [14] Y. Kim, Y. Li, and P. Panda, "One-stage prompt-based continual learning," in *European Conference on Computer Vision*. Springer, 2025, pp. 163–179.
- [15] Karthik, Maggie, and S. Dane, "Aptos 2019 blindness detection," <https://kaggle.com/competitions/aptos2019-blindness-detection>, 2019, kaggle.
- [16] T. Li, Y. Gao, K. Wang, S. Guo, H. Liu, and H. Kang, "Diagnostic assessment of deep learning algorithms for diabetic retinopathy screening," *Information Sciences*, vol. 501, pp. 511 – 522, 2019. [Online]. Available: <http://www.sciencedirect.com/science/article/pii/S0020025519305377>
- [17] E. Dugas, Jared, Jorge, and W. Cukierski, "Diabetic retinopathy detection," <https://kaggle.com/competitions/diabetic-retinopathy-detection>, 2015, kaggle.
- [18] L. Wang, X. Zhang, H. Su, and J. Zhu, "A comprehensive survey of continual learning: theory, method and application," *IEEE Transactions on Pattern Analysis and Machine Intelligence*, 2024.
- [19] J. Kirkpatrick, R. Pascanu, N. Rabinowitz, J. Veness, G. Desjardins, A. A. Rusu, K. Milan, J. Quan, T. Ramalho, A. Grabska-Barwinska *et al.*, "Overcoming catastrophic forgetting in neural networks," *Proceedings of the national academy of sciences*, vol. 114, no. 13, pp. 3521–3526, 2017.
- [20] F. Zenke, B. Poole, and S. Ganguli, "Continual learning through synaptic intelligence," in *International conference on machine learning*. PMLR, 2017, pp. 3987–3995.
- [21] B. Wang, X. Luo, and X. Zhuang, "Toward universal medical image registration via sharpness-aware meta-continual learning," in *International Conference on Medical Image Computing and Computer-Assisted Intervention*. Springer, 2024, pp. 739–748.
- [22] Q. Pham, C. Liu, and S. Hoi, "Continual normalization: Rethinking batch normalization for online continual learning," *arXiv preprint arXiv:2203.16102*, 2022.
- [23] S. Ebrahimi, F. Meier, R. Calandra, T. Darrell, and M. Rohrbach, "Adversarial continual learning," in *Computer Vision–ECCV 2020: 16th European Conference, Glasgow, UK, August 23–28, 2020, Proceedings, Part XI 16*. Springer, 2020, pp. 386–402.
- [24] M. Wortsman, V. Ramanujan, R. Liu, A. Kembhavi, M. Rastegari, J. Yosinski, and A. Farhadi, "Supermasks in superposition," *Advances in Neural Information Processing Systems*, vol. 33, pp. 15 173–15 184, 2020.
- [25] S.-A. Rebuffi, A. Kolesnikov, G. Sperl, and C. H. Lampert, "icarl: Incremental classifier and representation learning," in *Proceedings of the IEEE conference on Computer Vision and Pattern Recognition*, 2017, pp. 2001–2010.
- [26] P. Buzzega, M. Boschini, A. Porrello, D. Abati, and S. Calderara, "Dark experience for general continual learning: a strong, simple baseline," in *Advances in Neural Information Processing Systems*, H. Larochelle, M. Ranzato, R. Hadsell, M. F. Balcan, and H. Lin, Eds., vol. 33. Curran Associates, Inc., 2020, pp. 15 920–15 930.
- [27] C. Wu, L. Herranz, X. Liu, J. Van De Weijer, B. Raducanu *et al.*, "Memory replay gans: Learning to generate new categories without forgetting," *Advances in neural information processing systems*, vol. 31, 2018.
- [28] H. Shin, J. K. Lee, J. Kim, and J. Kim, "Continual learning with deep generative replay," *Advances in neural information processing systems*, vol. 30, 2017.
- [29] M. Oquab, T. Darcet, T. Moutakanni, H. Vo, M. Szafraniec, V. Khalidov, P. Fernandez, D. Haziza, F. Massa, A. El-Nouby *et al.*, "Dinov2: Learning robust visual features without supervision," *arXiv preprint arXiv:2304.07193*, 2023.
- [30] S. G. Kobat, N. Baygin, E. Yusufoglu, M. Baygin, P. D. Barua, S. Dogan, O. Yaman, U. Celiker, H. Yildirim, R.-S. Tan *et al.*, "Automated diabetic retinopathy detection using horizontal and vertical patch division-based pre-trained densenet with digital fundus images," *Diagnostics*, vol. 12, no. 8, p. 1975, 2022.
- [31] M. Boschini, L. Bonicelli, P. Buzzega, A. Porrello, and S. Calderara, "Class-incremental continual learning into the extended der-verse," *IEEE Transactions on Pattern Analysis and Machine Intelligence*, 2022.
- [32] Z. Wang, Z. Zhang, S. Ebrahimi, R. Sun, H. Zhang, C.-Y. Lee, X. Ren, G. Su, V. Perot, J. Dy *et al.*, "Dualprompt: Complementary prompting for rehearsal-free continual learning," in *European Conference on Computer Vision*. Springer, 2022, pp. 631–648.
- [33] A. Kirillov, E. Mintun, N. Ravi, H. Mao, C. Rolland, L. Gustafson, T. Xiao, S. Whitehead, A. C. Berg, W.-Y. Lo *et al.*, "Segment anything," in *Proceedings of the IEEE/CVF international conference on computer vision*, 2023, pp. 4015–4026.
- [34] J.-B. Alayrac, J. Donahue, P. Luc, A. Miech, I. Barr, Y. Hasson, K. Lenc, A. Mensch, K. Millican, M. Reynolds *et al.*, "Flamingo: a visual language model for few-shot learning," *Advances in neural information processing systems*, vol. 35, pp. 23 716–23 736, 2022.
- [35] B. Kim, C. Shin, J. Jeong, H. Jung, S.-Y. Lee, S. Chun, D.-H. Hwang, and J. Yu, "Zim: Zero-shot image matting for anything," *arXiv preprint arXiv:2411.00626*, 2024.
- [36] R. Singh, R. B. Puhl, K. Dhakal, and S. Sornapudi, "Few-shot adaptation of grounding dino for agricultural domain," *arXiv preprint arXiv:2504.07252*, 2025.
- [37] T. Ren, Y. Chen, Q. Jiang, Z. Zeng, Y. Xiong, W. Liu, Z. Ma, J. Shen, Y. Gao, X. Jiang *et al.*, "Dino-x: A unified vision model for open-world object detection and understanding, 2024," URL <https://arxiv.org/abs/2411.14347>, vol. 18, 2024.
- [38] Z. Wang, Z. Wu, D. Agarwal, and J. Sun, "Medclip: Contrastive learning from unpaired medical images and text," in *Proceedings of the Conference on Empirical Methods in Natural Language Processing. Conference on Empirical Methods in Natural Language Processing*, vol. 2022, 2022, p. 3876.
- [39] O. N. Manzari, H. Ahmadabadi, H. Kashiani, S. B. Shokouhi, and A. Ayatollahi, "Medvit: a robust vision transformer for generalized medical image classification," *Computers in biology and medicine*, vol. 157, p. 106791, 2023.